MRI Brain Extraction with Combined Expectation Maximization and Geodesic Active Contours

Albert Huang[1], Rafeef Abugharbieh[1], Roger Tam[2] and Anthony Traboulsee[2]

[1]Dept. of Elec. & Comp. Eng., The University of British Columbia, Vancouver, BC, V6T 1Z4, Canada
[2]Dept. of Medicine, The University of British Columbia, Vancouver, BC, V6T 1Z3, Canada

ABSTRACT

Abstract - *This paper presents a new fully automated method for the extraction of brain cortex from T1-weighted magnetic resonance imaging (MRI) head scans. Combined with the expectation maximization (EM) algorithm, and a hybrid of pre- and post-processing techniques, incorporating mathematical morphology and connected component analysis, geodesic active contours are evolved in 3D space to segment the cortex. The robustness and accuracy of our proposed method are validated with both synthetic and real MRI data. Our method outperforms standard techniques including the Brain Extraction Tool (BET) and Statistical Parametric Mapping (SPM) by lowering the misclassification rate, especially when analyzing real MRI data.*

Keywords – *magnetic resonance imaging (MRI), biomedical image processing, brain extraction*

I. INTRODUCTION

Extracting the brain cortex from T1-weighted magnetic resonance imaging (MRI) head scans is one of the important pre-processing steps in analyzing intracranial volumes. Any subsequent analysis, such as tissue segmentation or brain volume and atrophy measurement, will be highly dependent on the robustness and precision of the brain masks generated in the brain extraction step. By accurately defining the brain cortex, one could essentially minimize errors for the analyses that follow.

A number of techniques have been proposed for brain mask extraction from MRI data. A tessellated deformable sphere model has been used by Smith *et al.* [1] and is implemented in the popular Brain Extraction Tool (BET). Brain masks could also be generated indirectly by combining gray matter (GM) and white matter (WM) tissues segmented with tools such as Statistical Parametric Mapping (SPM) [2] which utilizes spatial templates and voxel-based morphometry for normalization and segmentation. BET and SPM perform well with synthetic data; however, results are poor and inconsistent (as observed in Section IV), when applied to real MRI scans. Shattuck *et al.* [3] developed a Brain Surface Extraction algorithm (BSE) based on mathematical morphology and connected component operations; however, BSE masks are often too smooth for standalone application as described in his paper. Lemieux *et al.* [4] used thresholding, Gaussian fitting, and connected component operations for this task but it had only been tested with synthetic data. Rehm *et al.* [5] offered a different approach by generating a consensus mask from an atlas-registered mask, a histogram-based mask and a BSE mask but the tool dependency and setup is too complex for practical use.

Our proposed method pre-processes T1-weighted MRI scans to generate inputs to a deformable model – namely a geodesic active contour. After the model converges to a stable solution, the mask is post-processed to further refine the perimeter of the brain cortex. The pre-processing and post-processing stages employ the expectation-maximization (EM) algorithm on a mixture of Gaussian models as well as mathematical morphology and connected component analysis.

II. METHOD

Our brain extraction algorithm starts by correcting for existing bias fields and noise artifacts. We apply the N3 bias field correction tool [6] and a Perona-Malik anisotropic diffusion filter [7] to our data before proceeding with the cortex extraction algorithm.

A. Review of Geodesic Active Contours

The geodesic active contours [8] framework transforms the energy minimization problem of an energy-based deformable model into finding the geodesic or the minimal distance curve in a Riemannian space by using a gradient descent search and the Euler-Lagrange equation. An initial curve C_0 is deformed according to the curve evolution equation:

$$\frac{\partial C}{\partial t} = g(I)(c+\kappa)\vec{N} - (\nabla g \cdot \vec{N})\vec{N} \qquad (1)$$

where κ is the Euclidean curvature, $\vec{N}$ is the inner unit

normal, g is some general function of the intensity I, c is a constant velocity term acting as a balloon force, and $\partial C/\partial t = \kappa\vec{N}$ is the Euclidean heat flow equation satisfying the geometric smoothing property [8]. Equation (1) can be embedded in a level-set of a function u as in (2), and then one searches for the steady state solution.

$$\frac{\partial u}{\partial t} = g|\nabla u|(c+\kappa) + \nabla g \cdot \nabla u \qquad (2)$$

The general function g acts as a feature function for determining the evolution and halting speed of the evolving curve, where a value of zero represents an ideal edge. Section II-B describes the feature function g for our proposed method.

B. Pre-processing

Before our geodesic active contour could be initialized in MRI scans, several pre-processing steps are necessary to ensure a stable convergence of the contour to the appropriate perimeter.

Non-brain Tissue Removal. Otsu [9] developed a threshold selection criterion by minimizing the interclass variance. We apply this threshold for brain and non-brain separation using a two-Gaussian mixture model (Fig. 1). We then apply another Otsu threshold to remove any significant high intensity clusters such as eyes and scalp from the brain region.

Using a basic peak searching strategy, our method automatically examines a low-pass filtered version of the resulting intensity histogram to determine if the GM/WM peaks are clearly distinguishable and separable before we fit two, in the case of low separability, or three Gaussian models using the EM algorithm. Once the Gaussian mixture parameters are determined, we then determine the initial contour and the feature image for the geodesic active contour evolution.

Initializing the Active Contour. The level-set approach requires an initial contour as the zero level-set from which the active contour then propagates. To choose a suitable contour inside the regions to be segmented, we choose the WM as the most confident region since its intensity is the highest on T1; therefore, better separability from the low intensity CSF is assured than if GM is used. The WM intensity range is determined based on minimal misclassification thresholding. If the WM and GM contrast is low, the entire WM/GM region is used instead of using only WM.

The resulting mask is further eroded with a 3D spherical structural element of a 1-pixel radius to remove edge regions that might have partial volume effects with the adjacent tissues. Pruning and connected component operations are then performed to ensure the initial contour is the largest connected component (Fig. 1).

Feature Image. The feature image from which the active contour derives its speed term and stopping function should be established based on a combined estimate of GM and WM. By using the Otsu threshold, we can easily determine the optimal threshold between GM/WM and CSF. A Gaussian smoothing is then used with 3mm variance to allow fuzzy edges for the contour evolution but without linking the desired anatomic brain region to other non-brain areas (Fig. 1).

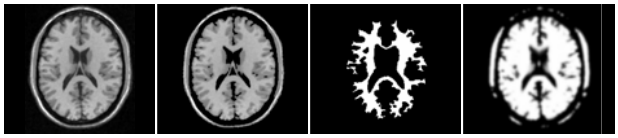

Fig. 1. Raw slice, foreground brain tissues with non-bran tissues removed, eroded WM estimate for contour initialization, smoothed GM/WM estimate for contour evolution feature (left to right).

C. Post-processing

After the geodesic active contour converges to a stable solution, the largest connected component is determined before further refinement is applied.

The EM Algorithm. The mask resulting from the active contour is dilated with a 3D spherical structural element of a 2-pixel radius to expand its coverage in order to compensate for our conservative model feature image described in Section II-B, and the resulting contour. Intensity thresholding is then performed with thresholds determined by fitting three Gaussian models to the intensity histogram using the EM algorithm. We retain tissues within three standard deviations of the lowest and the highest estimated means to include 99.7% of the GM and WM tissues and to remove any non-brain tissue.

Morphological Post-processing. A morphological opening operation is applied with a 1-pixel radius spherical structural element to untie any falsely linked tissues. Hole-closing is then performed in the axial, coronal and sagittal directions by finding the largest connected component in the background and filling those background pixels which do not belong to the largest connected background component.

III. DATA

For the simulated data tested, we used 18 synthetic volumes from the BrainWeb simulated brain database [10-13]. The T1-weighted modality data and the provided phantom are 1mm×1mm×1mm in spacing. Noise level varies

at 0%, 1%, 3%, 5%, 7% and 9%, and intensity non-uniformity varies at 0%, 20% and 40%.

For the real data tested, we used 18 real T1-weighted volumes which were acquired coronally with 256×256×128 in resolution and 1.5mm in thickness from the International Brain Segmentation Repository (IBSR V2.0). The MR brain data sets and their manual segmentations were provided by the Center for Morphometric Analysis at Massachusetts General Hospital and are available at http://www.cma.mgh.harvard.edu/ibsr/.

We also examined 15 clinical T1-weighted axial data from the MS/MRI Research Group at the University of British Columbia with 256×256×50 resolution and 0.937mm×0.937mm×3mm in spacing.

IV. RESULTS AND DISCUSSIONS

We evaluated both quantitative and qualitative results with the synthetic BrainWeb and real IBSR V2.0 data. Since no manual segmentation masks existed for the MS/MRI research group data, those were only qualitatively evaluated.

A. Quantitative Results

We compared the sensitivity (3) and specificity (4) of the 18 synthetic BrainWeb volumes with the provided phantom (Table I). T_+, T_-, F_+ and F_- represent true positive, true negative, false positive and false negative respectively.

$$Sensitivity = \frac{T_+}{(T_+ + F_-)} \qquad (3)$$

$$Specificity = \frac{T_-}{(T_- + F_+)} \qquad (4)$$

Since the BrainWeb phantom contains peripheral CSF, sensitivity is calculated based only on GM and WM, whereas specificity is calculated based on GM, WM and CSF. The SPM2 brain masks are determined by combining the segmented GM and WM with the intracranial regions filled.

TABLE I
AVERAGE PERFORMANCE OF 18 BRAINWEB VOLUMES

Method	Metric	Mean	Std Dev
SPM2	*Sensitivity*	*98.90%*	*0.45%*
	Specificity	*99.34%*	*0.10%*
BET	*Sensitivity*	*99.61%*	*0.05%*
	Specificity	*97.43%*	*0.23%*
Proposed Method	*Sensitivity*	*99.26%*	*0.10%*
	Specificity	*99.30%*	*0.11%*

Compared to SPM2, our proposed method outperforms in sensitivity and on average performs comparably in specificity. Compared to BET, our proposed method performs comparably in sensitivity and on average outperforms in specificity. In both cases, our method achieves low standard deviation values, thus, providing a more stable performance across all datasets.

We compared several additional metrics – similarity index (5), total misclassification (6) and volume difference (7), calculated from the 18 real IBSR V2.0 volumes with manual segmentation masks (Table II). We examined the F_- and F_+ ratio instead of sensitivity and specificity, because the provided data does not identify the brain/non-brain region in the MRI scans; thus, T_- information is not present.

$$SimilarityIndex = \frac{T_+}{\frac{1}{2}(2T_+ + F_+ + F_-)} \qquad (5)$$

$$TotalMisclassification = \frac{F_+ + F_-}{T_+ + F_-} \qquad (6)$$

$$VolumeDifference = \frac{|F_+ - F_-|}{T_+ + F_-} \qquad (7)$$

Compared to SPM2, our proposed method on average outperforms in every category. Compared to BET, our proposed method outperforms on average in every category except for F_-, and achieves much more significant stability with lower standard deviations. BET sacrifices F_+ for a lower F_- ratio. This result demonstrates that our proposed method is more conservative and potentially better suited for measuring the brain volumes.

TABLE II
AVERAGE PERFORMANCE OF 18 IBSR V2.0 VOLUMES

Method	Metric	Mean	Std Dev
SPM2	*Similarity Index*	*84.89%*	*6.87%*
	Misclassification	*28.95%*	*14.38%*
	Vol. Difference	*15.78%*	*7.59%*
	False Negative	*19.62%*	*7.25%*
	False Positive	*9.33%*	*12.47%*
BET	*Similarity Index*	*92.28%*	*5.32%*
	Misclassification	*17.29%*	*14.87%*
	Vol. Difference	*14.88%*	*14.41%*
	False Negative	*1.21%*	*1.35%*
	False Positive	*16.08%*	*14.58%*
Proposed Method	*Similarity Index*	*95.17%*	*2.50%*
	Misclassification	*9.33%*	*4.47%*
	Vol. Difference	*5.78%*	*5.08%*
	False Negative	*6.68%*	*5.35%*
	False Positive	*2.65%*	*1.83%*

B. Qualitative Results

We show the BrainWeb results in 2D and 3D (Fig. 2 and 3). Although both methods perform relatively well, our method produces a tighter brain mask than BET. This difference is also highlighted on the 3D renderings.

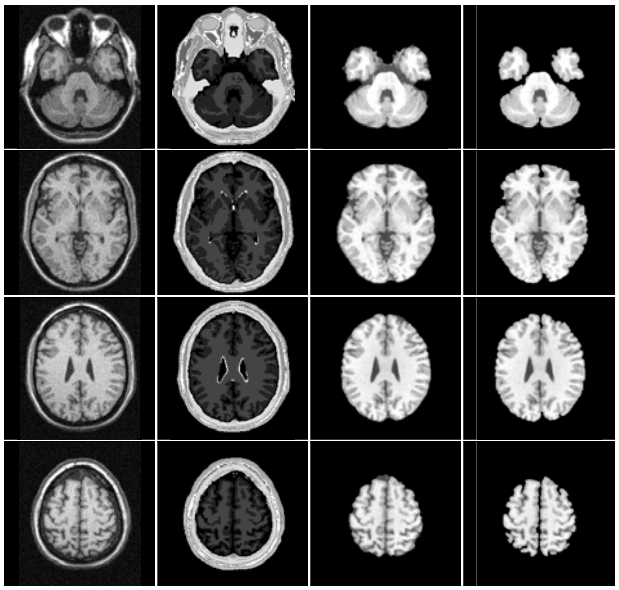

Fig. 2. Slices 40, 70, 100, and 130 (top to bottom) of a BrainWeb data, phantom, BET, and our results (left to right).

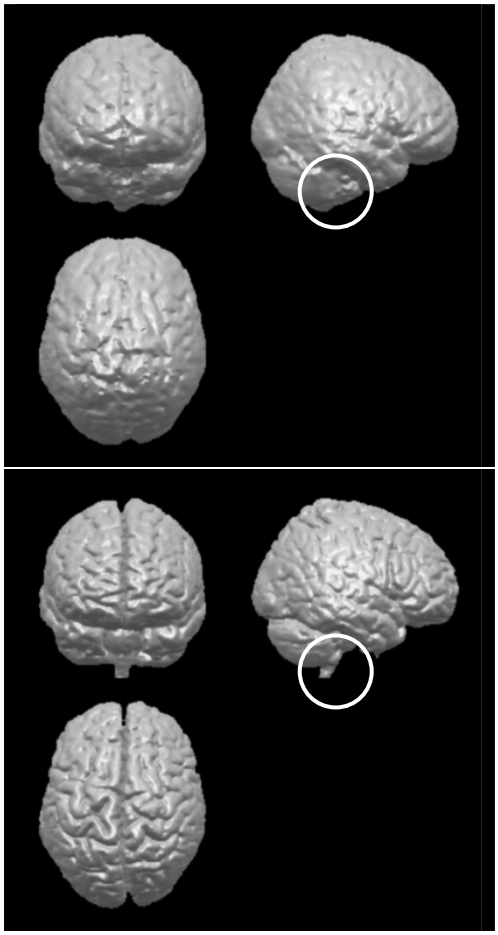

Fig. 3. 3D cortex rendering of BET (top) and our (bottom) results.

Next we examine the IBSR V2.0 results (Fig. 4), and observe similar findings. The highlighted regions indicate a closer match to the manual segmentation with our proposed method than with BET. Lastly, we compare the brain extraction performance when applying to clinical data from the MS/MRI Research Group (Fig. 5). BET fails to exclude the eye balls as highlighted, whereas our method does not.

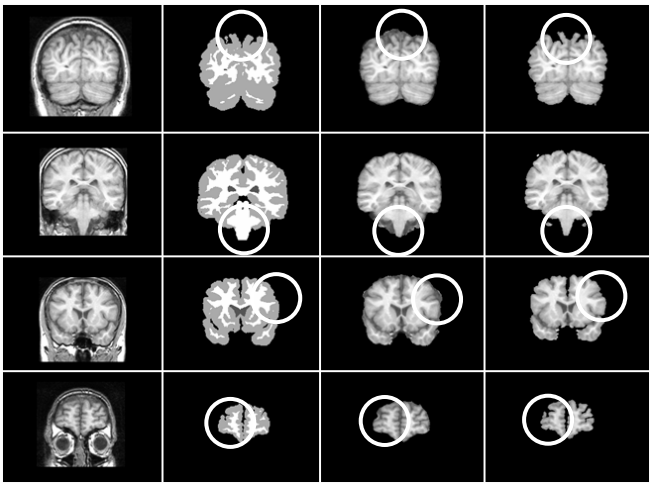

Fig. 4. Slices 20, 50, 80, and 110 (top to bottom) of IBSR V2.0 data, manual segmentation, BET, and our results (left to right).

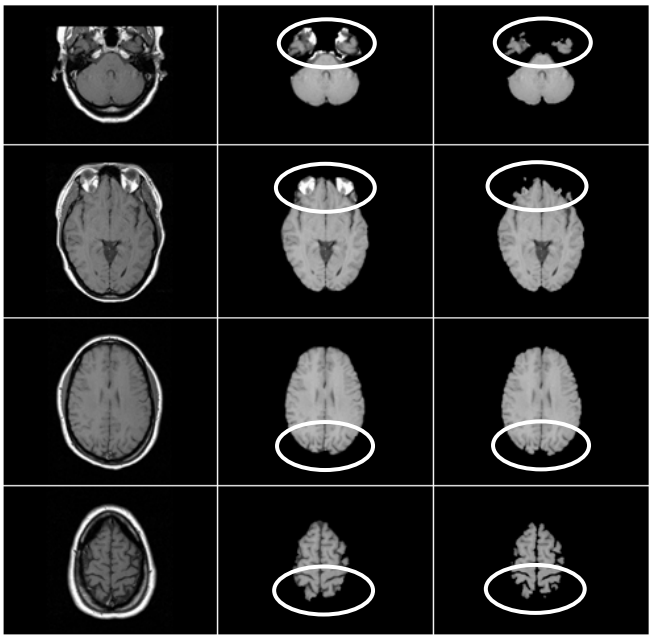

Fig. 5. Slices 10, 20, 30, and 40 (top to bottom) of MS/MRI data, BET, and our results (left to right).

Based on feedback from two expert radiologists and a neurologist at the MS/MRI Research Group, Depatrment of Medicine at the University of British Columbia, we validated that our brain extraction results match better qualitatively than BET to the manual segmentation masks.

V. CONCLUSION

We proposed a fully automatic method for extracting the brain cortex from the T1-weighted MRI head scans based on a hybrid of processing techniques including the EM algorithm and geodesic active contours. Our quantitative results show that against standard techniques such as SPM and BET, the proposed method achieves comparable performance with synthetic BrainWeb data, and significantly outperforms both techniques with real IBSR V2.0 data. Our results are also more consistent across the datasets, making the proposed method potentially better suited for measuring brain volumes in a clinical setting. Our qualitative results against BET show that the proposed method achieves a tighter brain mask around the brain cortex with both BrainWeb and IBSR V2.0 scans, and succeeds in removing problematic areas in the MS/MRI clinical scans.

REFERENCES

[1] S.M. Smith, "Robust Automated Brain Extraction," *Human Brain Mapping*, vol 17, no. 3, pp. 143-155, 2002.

[2] J. Ashburner and K.J. Friston "Voxel-based morphometry--the methods," *Neuroimage*, vol. 11, no. 6, pt. 1, pp. 805-821, 2000.

[3] D.W. Shattuck *et al.*, "Magnetic resonance image tissue classification using a partial volume model," *Neuroimage*, v. 13, no. 5, pp. 856-876, 2001.

[4] L. Lemieux *et al.*, "Fast, accurate, and reproducible automatic segmentation of the brain in T1-weighted volume MRI data," *Magn Reson Med*, vol. 42, no. 1, pp. 127-135, 1999.

[5] K. Rehm *et al.*, "Putting our heads together: a consensus approach to brain/non-brain segmentation in T1-weighted MR volumes," *Neuroimage*, vol. 22, no. 3, pp. 1262-1270, 2004.

[6] J.G. Sled *et al.*, "A non-parametric method for automatic correction of intensity non-uniformity in MRI data," *IEEE Transactions on Medical Imaging*, vol. 17, pp. 87-97, 1998.

[7] P. Perona and J. Malik, "Scale-space and edge detection using anisotropic diffusion," *IEEE Transactions on Pattern Analysis Machine Intelligence*, vol. 12, pp. 629–639, 1990.

[8] V. Caselles *et al.*, "Geodesic active contours," *International Journal of Computer Vision (IJCV)*, vol. 22, no. 1, pp. 61–79, 1997.

[9] N. Otsu, "A threshold selection method from gray level histograms," *IEEE Transactions on Systems, Man and Cybernetics*, v. 9, pp. 63–66, 1979.

[10] C.A. Cocosco *et al.*, "BrainWeb: Online Interface to a 3D MRI Simulated Brain Database," *NeuroImage*, vol. 5, no. 4, part 2/4, S425, 1997.

[11] R.K.-S. Kwan *et al.*, "MRI simulation-based evaluation of image-processing and classification methods," *IEEE Transactions on Medical Imaging*, vol. 18, no. 11, pp. 1085-97, November 1999.

[12] R.K.-S. Kwan, A.C. Evans, and G.B. Pike, "An Extensible MRI Simulator for Post-Processing Evaluation," *Visualization in Biomedical Computing (VBC'96)*. Lecture Notes in Computer Science, vol. 1131, pp. 135-140, Springer-Verlag, 1996.

[13] D.L. Collins *et al.*, "Design and Construction of a Realistic Digital Brain Phantom," *IEEE Transactions on Medical Imaging*, vol. 17, no. 3, pp. 463--468, June 1998.